Journal of
Electrical & Electronic Systems

Souhail et al., J Electr Electron Syst 2016, 5:3
DOI: 10.4172/2332-0796.1000196

Review Article Open Access

# From 2D to 3D Bifurcation Structures in Field Oriented Control of a PMSM

**Wahid Souhail[1]*, Hedi Khamari[2] and Mohamed Faouzi Mimouni[1]**

[1]*Electrical Engineering Department, National Engineering School of Monastir Monestir, Ibn al Jazar, Tunisia*
[2]*Computer Department, Faculty of Computer Science, Taief University Taief, Saudi Arabi*

**Abstract**

This paper presents new aspects of bifurcation structures in a Permanent Magnet Synchronous Machine (PMSM) in both motor and generator operating modes.

It considers the case where the PMSM speed is regulated with a Field-oriented control (FOC). A period doubling bifurcation cascade under the variation of a proportional control parameter leading to chaotic states, was identified.

The investigation of parametric singularities allows us to identify a complex bifurcation structure including three generic bifurcations. Such structure is made of the Limit Point (LP), the Hopf (H) and the Bogdanov-Takens (BT) bifurcation sets. Sufficient conditions of the existence of the main bifurcations are given analytically.

An overview of the phase space singularities associated to the parametric singularities is presented. Moreover, embedding 2D bifurcation sets in a 3D parametric space, led to identify certain bifurcation surface structures. The bifurcation surfaces established correspond to limit point bifurcation for the motor and generator operating mode, and for period doubling period bifurcation. The 3D bifurcation sets play an important role to study the combined effect of three different parameters on the PMSM dynamics, and permit to control the complex PMSM dynamics to a stable equilibrium dot by an adequate tuning of either control and system parameters.

**Keywords:** Bifurcation surface; Limit point; Hopf; Bogdanov-Takens; PMSM dynamics

**Abbreviations:** $\Omega$ : mechanical angular speed (rad/s); $i_{d,q}$ : direct and quadrature-axis currents (A); $V_{d,q}$ : direct and quadrature axis voltages (V); $T_L$ : load torque (N.m); $L_{d,q}$ : direct and quadrature-axis inductance (H); $R_s$ : stator winding resistance (ohm); $\phi_\phi$ : permanent magnet flux (wb); $f$ : viscous damping coefficient (N/rad/s); J: polar moment of inertia (kgm$^2$); p: number of pole pairs of the rotor; $k_p$ : proportional constant of current regulator; $k_i$ : integral constant of current regulator; $k_{pw}$ : proportional constant of speed regulator; $\grave{U}_{ref}$ : reference speed input; $i_{dref}$ : reference current input.

## Introduction

The permanent magnet synchronous motors (PMSM) are among the main preferences for industrial control applications. It has high power density, fast dynamic response and high efficiency. Because of its high reliability, the Field -oriented based controller (FOC) is mainly used for high dynamic performance induction motor drives.

For several industrial implementations, the speed regulation of the PMSM is ensured with such type of controllers [1].

Sustained oscillations may arise near equilibrium in PMSM due to the nonlinearities inherent to it. Many undesirable behaviors of PMSM were well documented, but little understood.

According to many studies, detection and suppression of undesirable behaviors namely chaos and sustained oscillations in PMSM are of high interest [2-6].

Power systems including electromechanical machines present several challenging problems related to the nonlinear characteristics of its components. The resulting physical behaviors, including bifurcation, chaos, resonance, voltage collapse, may cause the loss of stability and the transition from normal to anomalous operating regimes [7-9]. Bifurcation theory not only renders some machines' defaults more comprehensible but uncovers new problems that need research.

In attempts to study the dynamics of electric machines, the phase space singularities as well as the parametric singularities were studied in order to define the stability domains and to avoid the undesirable behaviors [2,4,5,10-13].

To overcome control draw backs and to solve the stabilization control problems in PMSM some control techniques were reported to be efficient enough to bring order to PMSM. The Lyapunov exponent based controller and the neural and back stepping techniques based nonlinear controllers were developed mainly to suppress chaos and to force the machine to a desired solution in an attraction basin [2-4,14-16]. In many nonlinear systems, Chaos can be originated from a succession of doubling period (Flip) bifurcations [17,18], these complex behaviors are usually twin. Thus not only chaos, but bifurcation control techniques are required for maintaining a system's behavior in a nominal operating state and to avoid loss of stability.

On the basis of parametric plane bifurcation structures, a qualitative characterization of bifurcation structure in 3D parametric space will be developed. This allows one to explore the eventual existence of generic characteristic bifurcation structures of PMSM behavior.

Among the objectives of this study, is to find bifurcation structures in 3D-parametric space which, on one hand give a global vision on the parameter effects on PMSM behavior, and, on the other hand, define

***Corresponding author:** Wahid Souhail, Electrical Engineering Department, National Engineering School of Monastir Monestir, Ibn al Jazar 5019, Tunisia, Tel: 73500515; E-mail: souhailwahid54@yahoo.fr

**Received** August 30, 2016; **Accepted** September 09, 2016; **Published** September 16, 2016

**Citation:** Souhail W, Khamari H, Mimouni MF (2016) From 2D to 3D Bifurcation Structures in Field Oriented Control of a PMSM. J Electr Electron Syst 5: 196. doi: 10.4172/2332-0796.1000196

normal operating domains of PMSM. For that purpose, one can start by detecting a bifurcations in a 2D-parameteric plane, and then embed it in a 3D-parameteric space by varying a third parameter. The resulting structure is a bifurcation surface.

The numerical continuation methods are the main tool used to plot the bifurcation diagrams and to explore the dynamics of the PMSM submitted to a FOC.

Section 2 is devoted to describe the system model and to define analytically the corresponding control model. Successive period doubling bifurcation leading to chaotic behavior is presented in section 3.

The section 4 is reserved to describe the existence conditions of three generic bifurcations, namely limit point (LP), Hopf (H) and Bogdanov-Takens (BT) bifurcations for particular sets of system and control parameters.

A different approach to characterize the PMSM dynamics, based on embedding a 2D-bifurcation structure into a 3D-parametric space is presented in section 5, and then the paper is ended by some concluding remarks.

## Mathematical Model of PMSM Drive System and Preliminaries

Consider a PMSM submitted to a Field Oriented Control (Figure 1).

The currents $i_a$, $i_b$ are measured with a current sensor. The Clarke transform is applied to determine the projection of stator current in a two coordinate non-rotating frame. Then its projection in the (d, q) rotating frame is performed via Park transform. The d, q projection of the stator phase currents are then compared to their reference values $i_{qref}$ and $i_{\mathrm{dref}} = 0$ and corrected by mean of PI current controllers. The outputs of the current controllers is transformed by an inverse Park transformation back from the d-q reference frame into the 2-phase system fixed with the stator which in turn is applied to the motor using the space vector modulation technique. Control of the motor speed is ensured by a reference current $i_{qref}$ generated by an outer loop.

The mathematical model of PMSM is given by:

$$\begin{cases} \dfrac{di_d}{dt} = \dfrac{-R_s}{L_d} i_d + \dfrac{pL_q}{L_d} i_q \Omega + \dfrac{1}{L_d} v_d \\ \dfrac{di_q}{dt} = \dfrac{-R_s}{L_q} i_q - \dfrac{pL_q}{L_q} i_d \Omega - \dfrac{p\phi_f}{L_q} \Omega + \dfrac{1}{L_q} v_q \\ \dfrac{d\Omega}{dt} = \dfrac{-f}{J} \Omega + \dfrac{p.m(L_d - L_q)}{2J} i_d i_q + \dfrac{p.m\phi_f}{2J} \Omega - \dfrac{T_L}{J} \end{cases} \quad (1)$$

For investigation of the control problem of the PMSM with smooth air gap, the direct and the quadratic-axis winding inductances are equal $(L = L_d = L_q)$

The PI regulator is defined by the expression:

$$u(t) = k_p \varepsilon(t) + k_i \int_0^t \varepsilon(t) dt \quad (2)$$

Where,

$$\varepsilon(t) = x_{ref} - x \quad (3)$$

The classical control method includes three PI regulators to generate the voltages $\mathrm{v_d}, \mathrm{v_q}$ having the following expressions:

$$v_d = k_p (i_{dref} - i_d) + k_i \int_0^t (\mathrm{i}_{dref} - \mathrm{i}_d) dt \quad (4)$$

$$v_q = k_p (i_{qref} - i_q) + k_i \int_0^t (\mathrm{i}_{qref} - \mathrm{i}_q) dt \quad (5)$$

The reference current $i_{qref}$ generated by the PI regulator of angular speed is given as:

$$\mathrm{i_{qref}} = \mathrm{k_{pw}} \left( \Omega_{\mathrm{ref}} - \Omega \right) + \mathrm{k_{iw}} \int_0^t \left( \Omega_{\mathrm{ref}} - \Omega \right) \mathrm{dt} \quad (6)$$

The integral regulators of the system are defined as:

$$\begin{aligned} S_{id} &= k_i \int_0^t (\mathrm{i}_{dref} - \mathrm{i}_d) dt \\ S_{iq} &= k_i \int_0^t (\mathrm{i}_{qref} - \mathrm{i}_q) dt \\ S_w &= k_{iw} \int_0^t (\mathrm{i}_{dref} - \Omega) dt \end{aligned} \quad (7)$$

The expression (6) becomes:

$$i_{qref} = k_{pw} (\Omega_{dref} - \Omega) + S_w \quad (8)$$

The input voltages are expressed as:

$$\begin{aligned} v_d &= k_p (i_{dref} - i_d) + S_{id} \\ v_q &= k_p [\mathrm{k}_{pw} (\Omega_{ref} - \Omega) + \mathrm{S}_w - i_q] + S_{id} \end{aligned} \quad (9)$$

Differentiating the equations (7) with respect to t, gives the following differential system:

$$\begin{aligned} \frac{dS_{id}}{dt} &= k_i (i_{dref} - i_d) \\ \frac{dS_{id}}{dt} &= k_i (k_{pw} \left( \Omega_{ref} - \Omega \right) + S_w - i_q) \\ \frac{dS_w}{dt} &= k_{iw} (\Omega_{ref} - \Omega) \end{aligned} \quad (10)$$

Then, the machine control model is described by a system of six differential equations:

$$\begin{cases} \dfrac{di_d}{dt} = -\dfrac{R_s + k_p}{L} i_d + p i_q \Omega + \dfrac{1}{L} S_{id} + \dfrac{k_p}{L} i_{dref} \\ \dfrac{di_q}{dt} = -\dfrac{R_s + k_p}{L} i_q - p i_d \Omega - \dfrac{p\phi_f + k_p k_{pw}}{L} \Omega \\ + \dfrac{1}{L} S_{iq} + \dfrac{k_p}{L} S_w + \dfrac{k_p k_{pw}}{L} \Omega_{ref} \\ \dfrac{d\Omega}{dt} = \dfrac{pm\phi_f}{2J} i_q - \dfrac{f}{J} \Omega - \dfrac{1}{J} T_L \\ \dfrac{dS_{id}}{dt} = k_i (i_{dref} - i_d) \\ \dfrac{dS_{iq}}{dt} = k_i \left( -i_q - k_{pw} \Omega + S_w + k_{pw} \Omega_{ref} \right) \\ \dfrac{dS_w}{dt} = k_{iw} \left( \Omega_{ref} - \Omega \right) \end{cases} \quad (11)$$

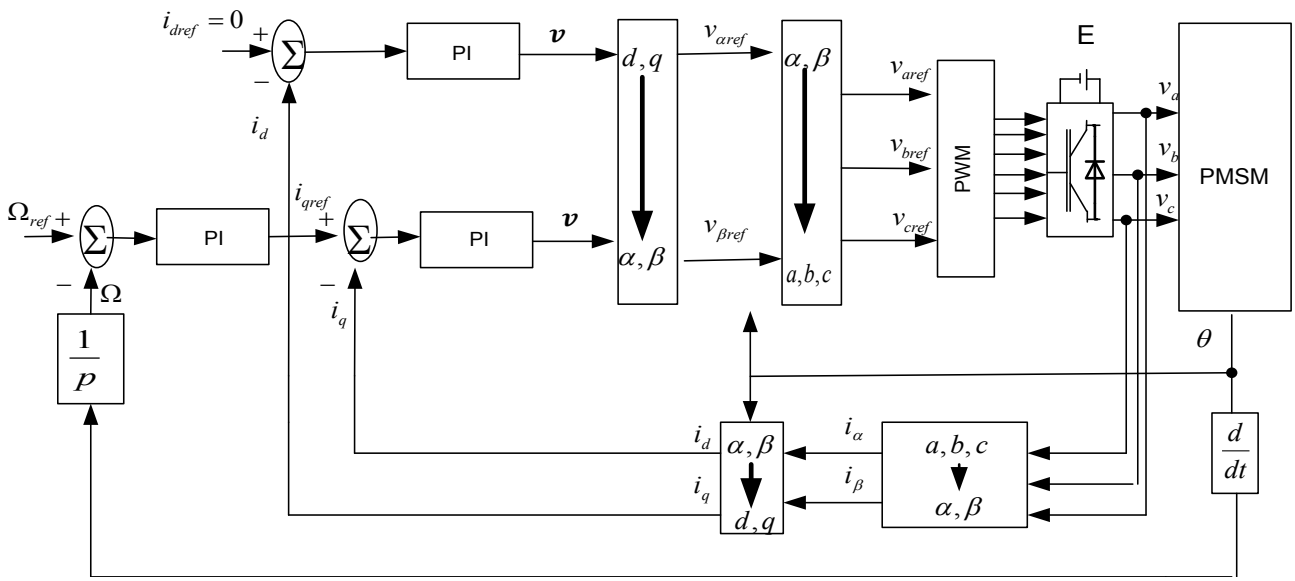


**Figure 1:** Schema of field oriented control of PMSM.

## Periodic Doubling Bifurcation and 'Route' to Chaos

### Computation of equilibrium points

The equation (11) can be written in the form:

$$\dot{X} = F(X) \tag{12}$$

With $X = (x_1, x_2, x_3, x_4, x_5, x_6) = (i_d, i_q, \Omega, S_{id}, S_{iq}, S_\omega)$ and $\dot{X} = dX / dt$

The equilibrium points are obtained *by equating the right-hand side* of the equation (12) to *zero as follows:*

$$\begin{aligned}
x_{e1} &= i_{dref} \\
x_{e2} &= \frac{2}{pm\phi_f}\left(f\Omega_{ref} + T_L\right) \\
x_{e3} &= \Omega_{ref} \\
x_{e4} &= \frac{\alpha R_s i_{dref} - L.p\left(f.\Omega_{ref} + T_L\right)\Omega_{ref}}{\alpha} \\
x_{e5} &= \frac{R_s(f\Omega_{ref} + T_L) + \alpha\Omega_{ref}(pLi_{dref} + p\phi_f)}{\alpha} \\
x_{e6} &= x_{e2}
\end{aligned} \tag{13}$$

With $\alpha = \frac{p.m.\phi_f}{2}$

The global stability and dynamic characteristics of the equilibrium point are profoundly affected by the parametric singularities namely the bifurcation phenomena that will be discussed in the next sections.

### Period doubling bifurcation of limit cycles

Analysis of the dynamical behavior of the PMSM led to identify a sequence of particular set of control bifurcation points. The transition from an equilibrium point to a limit cycle through a Hopf bifurcation is followed by a cascade of doubling period bifurcations (PD) which constitutes a veritable route to chaos.

A doubling period bifurcation occurs when a branch of period-doubled solutions is created or destroyed at the critical point. In the first case if the Hopf bifurcation is supercritical, a branch of stable period-doubled solutions emerges and the original stable periodic solutions will be continued as a branch of unstable periodic solutions. In the second case, if the Hopf bifurcation is subcritical, an unstable period-doubled solution is destroyed and then the stable periodic solutions evolve on a branch of unstable periodic solutions [8].

For the following conditions:

- input reference $\omega_{ref} = 100 rad.s^{-1}$, and $i_{dref} = 0A$
- The control parametres are $k_{pw} = 0.001$, $k_p = 0.25$, $k_i = 1$, $k_{iw} = 20$
- The load torque $T_{Ln} = 5N.m$

The machine has an equilibrium point $x_e$ = (0.015, 6.185,1 00, 1.682, 6.306, 6.245) with the eigenvalues : $\lambda_{1,2} = -0.0539 \pm j0.0528$, $\lambda_{3,4} = -0.0106 \pm j0.0097$, $\lambda_5 = -0.0026$, $\lambda_6 = -0.003$.

The continuation of this equilibrium point by varying $k_p$ led to a supercritical Hopf bifurcation at $k_p = 0.596$ with the eigenvalues:

$$\lambda_{1,2} = -0.00757 \pm j0.00428,\ \lambda_3 = -0.000899,$$

$$\lambda_4 = -0.000287,\ \lambda_{5,6} = \pm j0.00428.$$

Thus, the resulting limit cycle, with period T=9.33 s is stable and will undergo a cascade of period doubling bifurcation by decreasing $k_p$ Figure 2. As the parameter $k_p$ is varied, the machine enters into a complicated dynamics, through period doubling bifurcation, chaos intermittency and so on. Based on simulation results, the coordinates and the eigenvalues of the different PD bifurcation points are given in Table 1. It appears that in the PD critical points, two eigenvalues are equal to -1.

To make an overall inspection of the machine dynamics in different points of the bifurcation diagram, namely A, B, C, D, E, F, G, H and I, the phase portraits of the coordinate $x_1$ versus the variable $x_2$ are plotted in Table 2.

| Bif point | $k_p$ | Initial conditions | Eigenvalues |
|---|---|---|---|
| PD1 | 4.59196 | (-6.824, 2.423711,-1.84422, 0.0034, -0.0015, 1.004) | $\lambda_1=-1,\ \lambda_2=-1.000024,\ \lambda_{3,4}=0.0138\pm j0.0415,$ $\lambda_5=-0.0000227,\ \lambda_6=-0.000024$ |
| PD2 | 4.55175 | (-6.4432, 2.53505,-1.7974,0.003620,-0.0013, 1.0048) | $\lambda_1=-0.998,\ \lambda_2=-1,\ \lambda_{3,4}=0.0277\pm j0.0338,$ $\lambda_5=-0.0000227,\ \lambda_6=-0.000024v$ |
| PD3 | 4.55175 | (-7.2113, 2.3206,-1.9085, 0.003235,-0.0016, 1.0036) | $\lambda_1=-0.998,\ \lambda_2=-1,\ \lambda_{3,4}=0.0277\pm j0.0338,$ $\lambda_5=-0.0000227,\ \lambda_6=-0.000024$ |
| PD4 | 4.539713 | (-6.268,2.47,-1.78, 0.003651,-0.0012, 1.0049) | $\lambda_1=-0.998,\ \lambda_2=-1,\ \lambda_{3,4}=0.0274\pm j0.0335,$ $\lambda_5=-0.0000227,\ \lambda_6=-0.000024$ |
| PD5 | 4.539713 | (-6.64948, 2.5556,-1.8128, 0.003625,-0.0013,1.0048) | $\lambda_1=-0.998,\ \lambda_2=-1,\ \lambda_{3,4}=0.0274\pm j0.0335,$ $\lambda_5=-0.0000227,\ \lambda_6=-0.000024$ |
| PD6 | 4.539713 | X=(-7.21649, 2.3515,-1.9036,0.003331,-0.0015, 1.0038) | $\lambda_1=-0.998,\ \lambda_2=-1,\ \lambda_{3,4}=0.0274\pm j0.0335,$ $\lambda_5=-0.0000227,\ \lambda_6=-0.000024$ |
| PD7 | 4.539713 | X=(-7.27319,2.2835,-1.9234,0.003149,-0.0016, 1.0033) | $\lambda_1=-0.998,\ \lambda_2=-1,\ \lambda_{3,4}=0.0274\pm j0.0335,$ $\lambda_5=-0.0000227,\ \lambda_6=-0.000024$ |

**Table 1:** Coordinates of the PD bifurcations points.

## Existence Conditions of Certain Parametric Singularities

Some control approaches reset the Integral action of the PI when the Saturation is reached and particularly the anti wind up methods based on removing the integral part from the input [19].

The integral correctors of the machine drive have an important effect on the system dynamics. The case of a machine driver without integral correctors is considered, so the mathematical model of system given in (11) can be transformed as:

$$\begin{cases}\dfrac{di_d}{dt}=\beta_1 i_d+i_q\omega+g_1\left(i_{dref}\right)\\ \dfrac{di_q}{dt}=\beta_1 i_q-i_d\omega+\beta_2\omega+\ g_2\left(\omega_{ref}\right)\\ \dfrac{d\omega}{dt}=\gamma i_q+\varepsilon T\end{cases}\qquad(14)$$

With:

$$\omega=p\Omega$$

$$\beta_1=-\frac{R_s+k_p}{L},k_p>0$$

$$\beta_2=-\frac{p\phi_f+k_pk_{pw}}{L},k_{pw}>0$$

$$g_1\left(i_{dref}\right)=\frac{k_p}{L}i_{dref}$$

$$g_2\left(\omega_{ref}\right)=\frac{k_pk_{pw}}{L}\omega_{ref}=k_2$$

With:

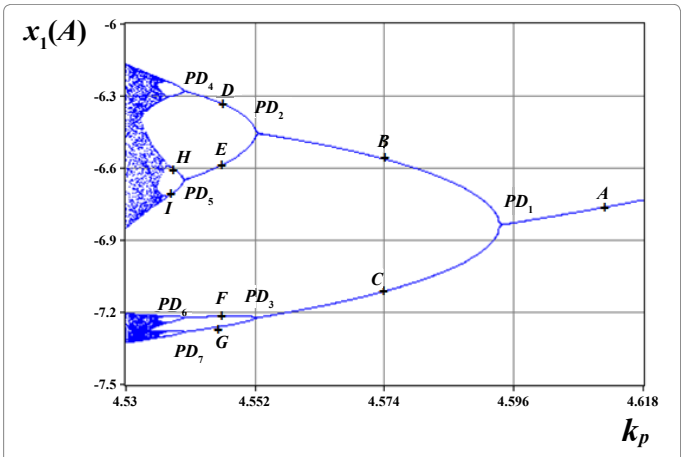


**Figure 2**: Bifurcation diagram of $x_1$ versus $k_p$: Sequence of period doubling and route to chaos.

$$\varepsilon=-\frac{p}{f},\gamma=\frac{p^2m\phi_f}{2J},\omega_{ref}=p\Omega_{ref}$$

For graphs, let $k_2$ parameter denote the function $g_2(\omega_{ref})$

The Jacobian matrix of the system (14) is defined as:

$$J\left(x_e\right)=\begin{pmatrix}\beta_1 & x_{e3} & x_{e2}\\ -x_{e3} & \beta_1 & \beta_2-x_{e1}\\ 0 & \gamma & 0\end{pmatrix}\qquad(15)$$

The characteristic polynomial of Jacobian matrix is:

$$p\left(\lambda\right)=\det\left(J\left(x_e\right)-\lambda I\right)\qquad(16)$$

$$p\left(\lambda\right)=-\lambda^3+tr\left(J\left(x_e\right)\right)\lambda^2+p_1\lambda+\det\left(J\left(x_e\right)\right)=0\qquad(17)$$

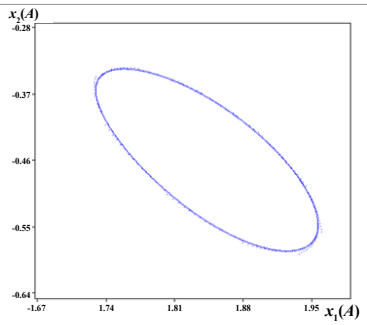

a. A = (-6.76,2.41, -1.84,0.0035, -0.00153,1.004)
kp=4.609- Stable- 1T

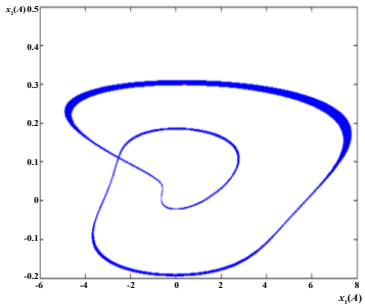

b. B = (-6.5,2.5,-1.81, 0.00348,-0.00139,1.0045)
kp=4.574- Stable-2T

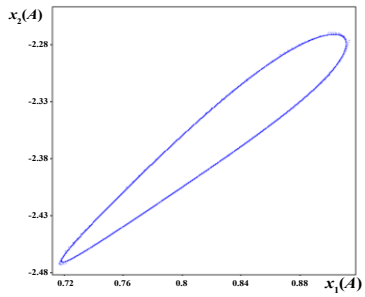

c. C = (-7.1,2.37,-1.88, 0.00328,-0.00160,1.00368)
kp=4.574- Unstable-1 T

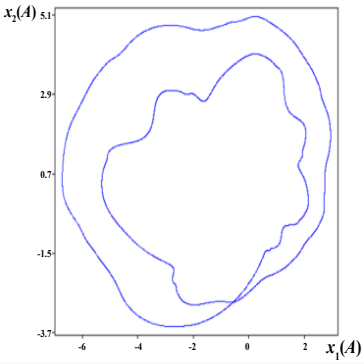

d. D = (-6.59,2.517, -1.81, 0.00361,-0.0013,1.00495)
kp = 4.546-Unstable-2T

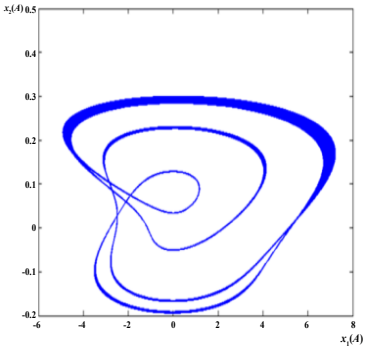

e. E = (-6.37,2.54, -1.795, 0.003645,-.00132,1.00495)
kp = 4.546-Stable-4T

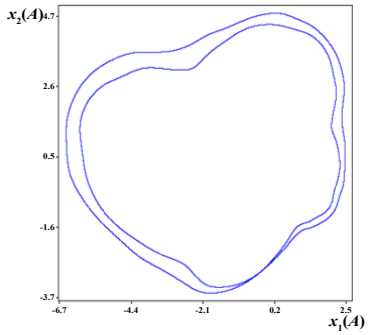

f. F = (-7.305,2.32,-1.91, 0.00317,-0.00168, 1.00355)
kp = 4.546-Unstable-2T

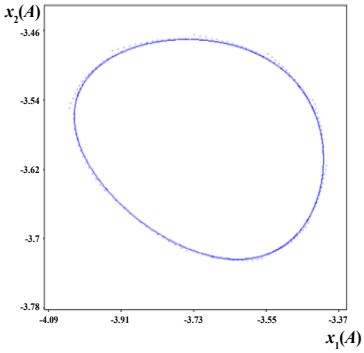

g. G = (-7.25,2.28,-1.92, 0.00317,-0.00168,1.0035)
kp=4.546-Stable-T

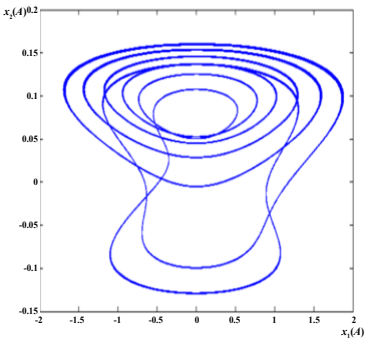

h. H = (-6.6,2.54,-1.81, 0.00365,-0.00132,1.0049)
kp= 4.539713- Stable-8 T

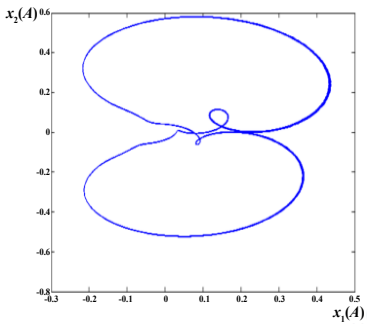

i. I=(-6.8,2.53,-1.8,0.0036,-0.00133,1.00482)
kp= 4.539713- Unstable-4 T

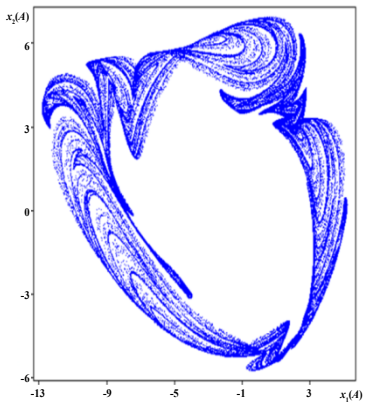

$X_{01} = (-7.3, 2.3, -1.8, 0.00334, -0.00163, 1.0037)$ $k_p = 4.53$ - Chaos

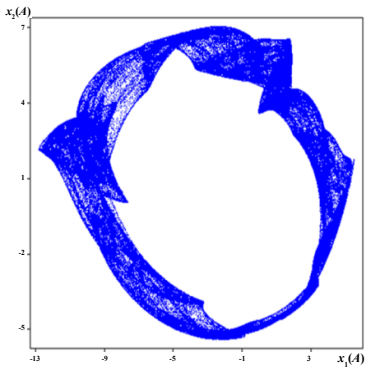

$X_{02} = (-6.3, 2.55, -1.9, 0.00362, -0.00129, 1.0049)$ $k_p = 4.53$ - Chaos

**Table 2**: Phase portraits in phase plane $x_1 - x_2$ for different values of $k_p$ .

Where,

$tr\left(J\left(x_e\right)\right)=2\beta_1, p_1=-\beta_1^2+\gamma\left(\beta_2-x_{e1}\right)-{x_{e3}}^2$

and

$det(J\left(x_e\right))=-\gamma\left(\beta_2-x_{e1}\right)\beta_1-\gamma x_{e2}x_{e3}$

Preliminary results on existence conditions of three bifurcation types sets for certain sets of PMSM and control parameters are determined in the following subsections.

### Limit point bifurcation

Investigation was conducted to establish the conditions leading to limit point bifurcation. The LP bifurcation, which results from interaction between stable and unstable equilibrium points, has three eigenvalues, one of which is 0 and two are nonzero. Therefore, the necessary existence conc ition is derived from the equation $p(\lambda)=0$, by taking $\det\left(J\left(x_e\right)\right)=0$ , therefore the roots of the characteristic polynomial are expressed as:

$\lambda_1=0$ and $\lambda_{2,3}=\frac{tr\left(J\left(x_e\right)\right)\pm\sqrt{\Delta_1}}{2}$ such as $\Delta_1=tr\left(J\left(x_e\right)\right)^2+4p_1$

Now, the detection of fold bifurcation point needs to search the roots of the determinant equation.

$$det(J\left(x_e\right)=-\gamma\left(\beta_2-x_{e1}\right)\beta_1-\gamma x_{e2}x_{e3}=0 \quad (18)$$

$$\beta_1=\frac{-x_{e2}x_{e3}}{\beta_2-x_{e1}}$$

With

$\beta_2\neq x_{e1}$

### Hopf bifurcation

A Hopf bifurcation occurs when two complex eigenvalues cross through the imaginary axis while the other eigenvalues are in the open left-hand side of the complex plane.

The Routh-Hurwitz stability criterion is applied to polynomial $p(\lambda)$ , in order to derive the condition for existence of Hopf bifurcation [13] (Table 3).

$$\text{With } q\left(\beta_1\right)=\frac{\det\left(J\left(x_e\right)\right)+p_1tr(J\left(x_e\right))}{tr(J\left(x_e\right))} \quad (19)$$

Such condition is stated as:

$q\left(\beta_1\right)=0, tr\left(J\left(x_e\right)\right)<0$ , and $\det\left(J\left(x_e\right)\right)<0$

Then,

$$\beta_2=\frac{2\beta_1^3-\left(2{x_{e3}}^2-\gamma x_{e1}\right)\beta_1+\gamma x_{e2}x_{e3}}{\gamma\beta_1} \quad (20)$$

Where,

$\beta_1>\frac{x_{e2}x_{e3}}{\left(\beta_2-x_{e1}\right)}$ with $\beta_2<x_{e1}$

### Bogdanov-Takens bifurcation

The Bogdanov-Takens bifurcation (BT) is a local codimension 2 bifurcation of an equilibrium point. In the parameter plane, the critical equilibrium has a zero eigenvalue of multiplicity two. For near parameter values, the system has a saddle and a non-saddle points which collide and disappear via a saddle node bifurcation. The non-saddle equilibrium turns into a limit cycle when it crosses an Andronov-Hopf bifurcation H. This cycle changes into an orbit homoclinic to the saddle and vanishes via a saddle homoclinic bifurcation [6].

Looking for the possible existence of double-zero eigenvalues of the Jacobian matrix (18), the necessary condition for the occurrence of such a bifurcation is:

$$\begin{cases}\det\left(J\left(x_e\right)\right)=0\\ p_1=0\end{cases}$$

Then the characteristic polynomial becomes:

$$p\left(\lambda\right)=\lambda^2(tr\left(J\left(x_e\right)\right)-\lambda) \quad (21)$$

The eigenvalues are $\lambda_{1.2}=0$ and $\lambda_3=2\beta_1<0$

The existence of Bagdanov-Takens bifurcation BT is controlled by the condition:

$$\beta_2=\frac{\beta_1^2+\gamma x_{e1}+x_{e3}(x_{e3}-\gamma x_{e2})}{\gamma(\beta_1+1)}$$

Thus,

$$\beta_2=\frac{\beta_1^2+c}{\gamma(\beta_1+1)} \quad (22)$$

With,

$c=\gamma x_{e1}+x_{e3}(x_{e3}-\gamma x_{e2})$

## Bifurcation Structure Analysis

Using bifurcation calculations one can divide a two-parameter plane into a number of regions, for which there are qualitatively different dynamics. This paves the way to classify and further investigate the dynamical behavior in each of these regions.

### Machine operation under overload mode ($T_L > T_{Ln}$)

For a load torque $T_L=10N.m$ and starting from the initial condition $x_i=(1,1,1)$, the trajectories of state variables converge to the equilibrium point: $x_e=(-2.45,8.1,73.76)$ where the inputs of the system $g_1(x)=-38.61$ and $g_2(x)=-204$. Fixing the parameter of system at $\beta_1=-5$ and $\beta_2=-10$ , the eigenvalues of this equilibrium point are $\lambda_1=-111.78,\ \lambda_{2,3}=-44.6\pm j601.48$. (Figure 3) displays the parameter plane in which the system behavior is investigated in different areas. The Bogdanov-Takens bifurcation point is detected for $\beta_1=-10$ and $\beta_2=-3.83$. The corresponding eigenvalues are $\lambda_2=\lambda_3=0$ and $\lambda_3=-21$. The area 2 presents an unstable dynamical behavior of the system where three eigenvalues are positives.

The limit point curve $Lp^+$ is controlled by $\lambda_2=0$, $\lambda_1$ is negative and $\lambda_3$ is in the right half of the complex plane. The corresponding behavior is anunstable equilibrium point which appears also in areas 2' and 2". The areas 2 and 2' are separated by a limit point curve $Lp^+$.

| | | |
|---|---|---|
| $\lambda^3$ | -1 | $p_1$ |
| $\lambda^2$ | $tr(J\left(x_e\right))$ | $det(J\left(x_e\right))$ |
| $\lambda^1$ | $q(\beta_1)$ | 0 |
| $\lambda^0$ | $det(J\left(x_e\right))$ | 0 |

**Table 3:** Routh-Hurwitz criterion.

The areas 1' and 1 which are characterized by a stable equilibrium point, are delimited by a Limit Point curve $Lp^-$ (the eigenvalues $\lambda_1, \lambda_2$ are negatives and $\lambda_3 = 0$), a Hopf bifurcation curve H ($\lambda_2$, $\lambda_3$ are purely imaginary and $\lambda_1$ is negative) and a zero neutral saddle curve NS. Each point of such bifurcation curve has one eigenvalue equal zero $\lambda_1 = 0$ and two opposite eigenvalues $\lambda_2 + \lambda_3 = 0$ [20].

## Machine Operation for $(T_L \le T_{Ln})$

Now, if the system parameters are changed to $\beta_1 = -100$, $\beta_2 = -46.66$, $\gamma = 8100$ and starting from the same initial point $x_i = (1,1,1)$, the machine will tend to the equilibrium point $EP: x = (-0.99, 0, 2.18)$ and the inputs of the motor will be $g_1(x) = -100$, $g_2(x) = 100$, $T_L = 2N.m$ and the eigenvalues of the Jacobian matrix are $\lambda_1 = -339.33$ and $\lambda_{2,3} = -170,22 \pm j584.29$.

**One parameter bifurcation diagram:** Varying the parameter $\beta_1$, limit point bifurcations are detected and displayed in ($\beta_1, x_1$) plane (Figure 4).

The type of bifurcation point is detected at $\beta_1 = -10.1$ with the eigenvalues $\lambda_{1,2} = -10.5 \pm j129.02$ and $\lambda_3 = 0$ and an equilibrium point $x = (-2.42, -0.019, 73.76)$.

In (Figure 5), taking the load torque $T_L$ as a bifurcation parameter, four bifurcations of type LP are detected in $(T_L, x_1)$ plane (Table 4).

**Two-parameter bifurcation plane:** The continuation of the limit points $LP_{10}$ and $LP_{11}$ in the parameter plane $(\beta_1, k_2)$ permits to trace limit point bifurcation curves for motor $(T_L = 5.59N.m)$ and generator $T_L = -4.78N.m$ operating modes, (Figure 6).

Both curves contain a branching point (BP) and a Bogdanov-Takens bifurcation points.

For the motor operating mode the branch point is:

$BP: x = (-5.09, 6.9, -31.48), (\beta_1, k_2) = (-62.28, 320)$

and the eigenvalues are $\lambda_{1,2} = -62.78 \pm j170.78$, $and \lambda_3 = 0$. In this singular point two equilibrium points collide and disappear and there is no unique tangent, which results in speed control lost. The Bogdanov-Takensfor the same operating mode is $BT: x = (-3.71, 6.9, 0.33)$, $(\beta_1, k_2) = (-26.31, 181.72)$ and the eigenvalues are $\lambda_1 = -53.63$, $\lambda_2 = -0.00073$, $\lambda_3 = 0.00073$. In this point the motor tends to reverse rotation and continues to spin at low speed $x_3 = 0.33 rad/s$.

For generator operating mode, the same types of bifurcations are shown in an apparent symmetry on the LP bifurcation curve.

**Effect of the variation of a third parameter on the bifurcation sets:** More features of the bifurcation structure displayed in a parameter plane could be revealed by varying a third parameter. In the parameter plane $(k_p, k_2)$, a set of LP bifurcation curves are computed for different values of $k_p$ and for both operating modes (Figure 7). The coordinates of branch points and Bogdanov-Takens bifurcation for a motor operating mode are given in (Tables 5 and 6).

Embedding the bifurcation structure shown in Figure 8 into the parametric space $(\beta_1, k_2, k_p)$ (Figure 8a). A qualitative 3D representation of the LP bifurcation curves for each of the motor operating mode (blue) and the generator operating mode (green), shows a parabolic shaped surface in the parametric space $(\beta_1, k_2, k_p)$.

Each bifurcation surface includes, for each operating mode, a Branch Point bifurcation curve (red dashed line) and a Bogdanov-Takens bifurcation curve (black dashed line). The continuity of the transitions between the LP bifurcation curves is let to be proved in further researches. The LP bifurcation curves under the variation of $k_p$ form a 3D parabolic shaped surface concave to the left for motor operating mode and concave to the right for generator operating mode (Figure 8b).

A similar analysis is applied to determine a period doubling bifurcation surface. Starting from a set of closed PD bifurcation curves for different values of $k_{iw}$, traced in the parametric space $(k_p, k_i, k_{iw})$, a qualitative 3D closed PD bifurcation surface is derived, see Figures 10 and 11 respectively. The construction of bifurcation surface is introduced, in order to put forward a new formalism related to bifurcation structure in 3D parametric space. As a bifurcation point of codimension 1 map to a bifurcation curve in parameter plane, the latter maps to a surface in 3D parametric space. A codimension two

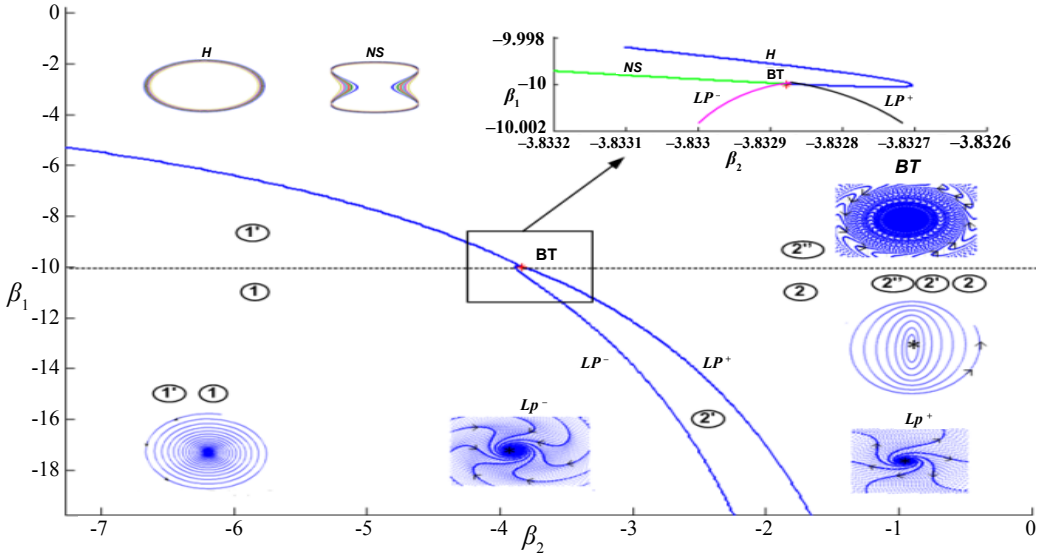


**Figure 3:** Parametric singularities in $\beta_1 - \beta_2$ plane.

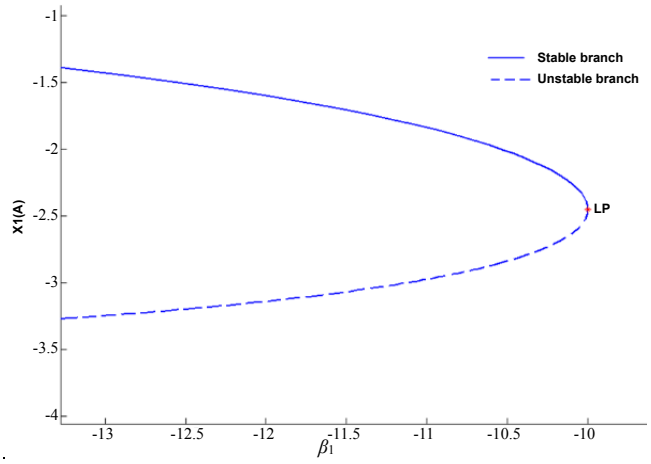


**Figure 4:** Bifurcation diagram in $\beta_1 - x_1$ plane.

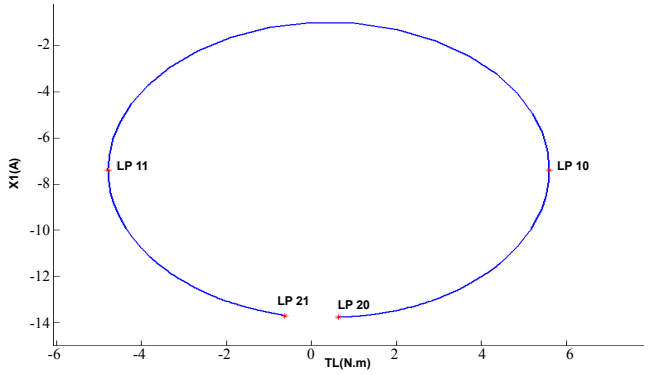


**Figure 5:** Bifurcation diagram in $T_L - x_1$ plane.

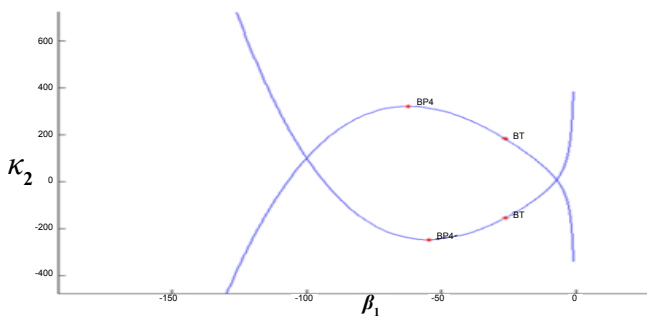


**Figure 6:** LP bifurcation curves for motor and generator operating mode.

bifurcation point in parameter plane, maps to a bifurcation curve in 3D parameter space. Based on the results obtained in Figure 8 and under realistic assumptions, the 3D parameter space can be considered as a set of codimension one bifurcation surfaces connected through codimension two bifurcation curves. This study paves the way to further researches aiming to explore more generic structures of bifurcation surfaces in 3D parametric space and to study the effect of varying a fourth parameter on their shapes and sizes. Also the study aims to strengthening the knowledge and practice on the combined effect of a broader set of parameters on the PMSM dynamics (Figures 9 and 10).

## Conclusion

The simulation results not only can reveal the dependence of PMSM behavior on the control parameters, but also it can be used for control and design purposes. Methods from bifurcation theory are applied to identify and characterize complex bifurcation sets of PMSM behavior in both motor and generator operating modes.

After identifying a period doubling bifurcation cascade under the variation of a proportional control parameter, the analytical necessary conditions for existence of Hopf and Bogdanov-Takens and limit point bifurcations are given in this paper. These parametric space singularities permit to understand the mechanism of transition from equilibrium dot to limit cycle and from one limit cycle to another limit cycle with different order and stability.

Embedding 2D bifurcation structures into 3D bifurcation ones is mainly introduced to study the combined effect of a larger set of parameters on the PMSM dynamics and to widen the understanding of certain types of parametric and phase space singularities.

The bifurcation surfaces established correspond to limit point bifurcation for the motor and generator operating mode, and for period doubling period bifurcation.

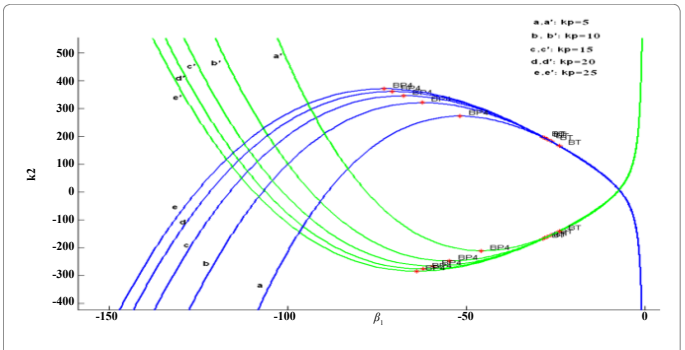


**Figure 7:** LP bifurcation curves for different $k_p$.

| | $T_L$ | Eigenvalues | Neighboring equilibrium point |
|---|---|---|---|
| $LP_{10}$ | $T_L = 5.59N.m$ | $\lambda_{1,2} = -100.5 \pm j245.4,\ \lambda_3 = 0$ | $x = (-7.38, 6.89, -92.63)$ |
| $LP_{11}$ | $T_L = -4.78N.m$ | $\lambda_{1,2} = -100.5 \pm j251.73,\ \lambda_3 = 0$ | $x = (-7.38, -6.89, 108, 37)$ |
| $LP_{20}$ | $T_L = 0.64N.m$ | $\lambda_{1,2} = -100.5 \pm j3216.8,\ \lambda_3 = 0$ | $x = (-13.76, 0.39, -3216.81)$ |
| $LP_{21}$ | $T_L = -0.64N.m$ | $\lambda_{1,2} = -100.5 \pm j3201.13,\ \lambda_3 = 0$ | $x = (-13.7, -0.39, 3201)$ |

**Table 4:** Limit points: These points can be used as starting points for tracing bifurcation curves in any parameter plane including $T_L$.

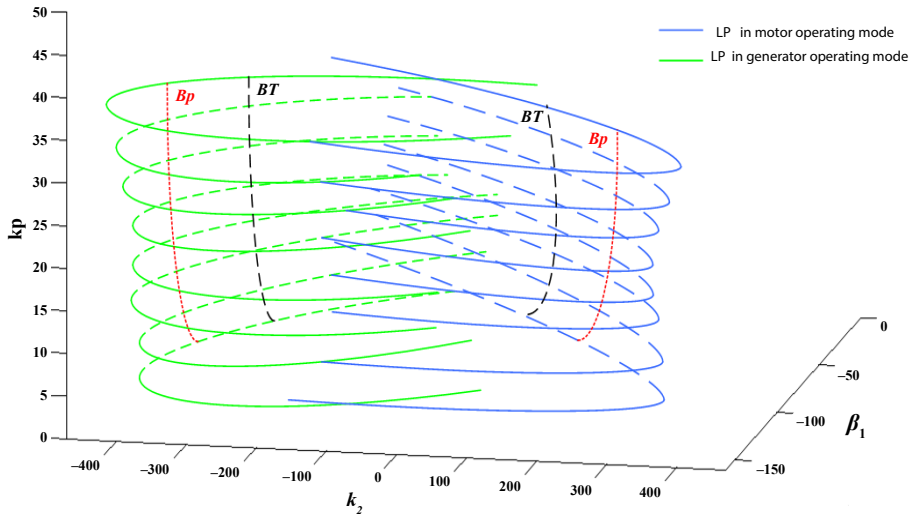


**Figure 8a**: Dynamical behavior of PMSM in 3D parameter space.

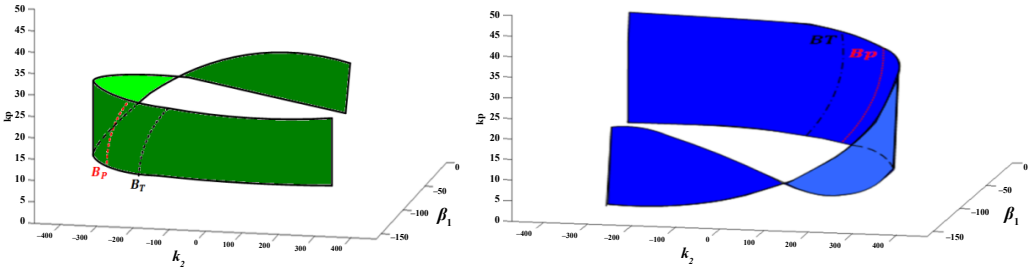


Generator operating mode

Motor operating mode

**Figure 8b:** Qualitative structure of LP bifurcation surface.

| $k_p$ | 5 | 10 | 15 | 20 | 25 | 30 | 35 | 40 |
|---|---|---|---|---|---|---|---|---|
| $k_2$ | 271.87 | 320.65 | 345.42 | 360.42 | 370.48 | 377.69 | 383.115 | 387.34 |
| $\beta_1$ | -51.92 | -62.32 | -67.62 | -70.83 | -72.99 | -74.54 | -75.54 | -76.61 |

**Table 5:** Branch point bifurcation coordinates.

| $k_p$ | 5 | 10 | 15 | 20 | 25 | 30 | 35 | 40 |
|---|---|---|---|---|---|---|---|---|
| $k_2$ | 165.52 | 181 | 189.28 | 193.66 | 196.52 | 198.54 | 200.103 | 201.19 |
| $\beta$ | -23.97 | -26.31 | -27.41 | -28.048 | -28.46 | -28.75 | -28.97 | -29.14 |

**Table 6:** Bogdanov-Takens bifurcation coordinates.

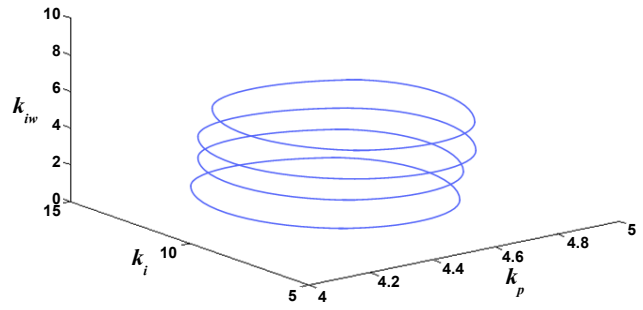


**Figure 9:** PD bifurcation curves for different $k_{iw}$.

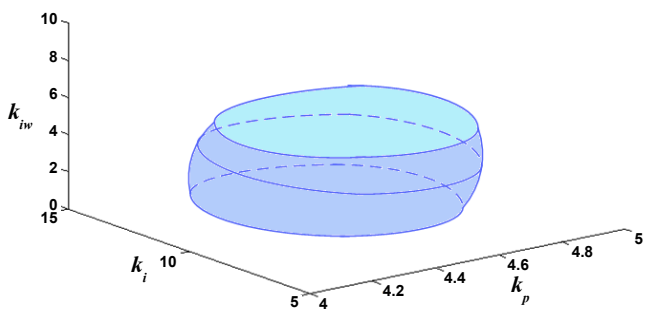


**Figure 10:** Closed PD bifurcation surface.

## References

1. Bhardwaj M (2013) Sensored field oriented control of 3-phase permanent magnet synchronous motors. Texas Instruments, application report SPRABQ2.
2. Huang G, Wu X (2011) Hopf bifurcation of permanent-magnet synchronous motor chaos system. International Conference on Computational and Information Sciences, Chengdu, China.
3. Dan Z, Fuzhong W, Heli H (2010) Adaptive stabilization control of non-smooth-air-gap PMSM chaotic systems with uncertain parameters. Proceedings of the 29th Chinese control conference, Beijing, China.
4. Li Z, Park JB, HoonJoo Y, Zhang B, Chen G (2002) Bifurcations and chaos in permanent-magnet synchronous motor. Fundamental Theory and Application 49: 383-387.

5. Ren H, Liu D (2006) Nonlinear feedback control of chaos in permanent magnet synchronous motor. IEEE transactions on circuit and system society.
6. Salas F, Reginatto R, Gordillo F, Aracil J (2004) Bogdanov-Takens bifurcation in indirect field oriented control of induction motor drives. 43rd IEEE Conference on Decision and Control, Atlantis, Paradise Island, Bahamas.
7. Chin-Woo T, Matthew V, Varaiya P, Felix F (1995) Bifurcation, chaos, and voltage collapse in power systems. Proceedings of the IEEE 83: 1484 - 1496.
8. Jing C, Xu D, Chang Y, Chen L (2003) Bifurcation, chaos, and system collapse in a three node power system. International Journal of Electrical Power and Energy Systems 25: 443-461.
9. Harb AM, Widyan MS (2002) Controlling chaos and bifurcation of sub synchronous resonance in power system. Nonlinear analysis: Modelling and Control 7: 15-36.
10. Jabli N, Khammari H, Mimouni MF, Aljahdali S (2013) Stability margins and low-codimension bifurcations of indirect field oriented control of induction motor. International transaction of electrical and computer engineers system 1: 6-14.
11. Chen G, Moiola JL, Wang HO (2000) Bifurcation control: theories, methods, and application. International Journal of Bifurcation and Chaos 10: 511-548.
12. Jabli N, Khammari H, Mimouni MF, Dhifaoui R (2010) Bifurcation and chaos phenomina appearing in induction motor under variation of PI controller parameters. WSEAS Transactions on systems 9: 784-793.
13. Jabli N, Khammari H, Mimouni MF, Dhifaoui R (2010) An analytical study of low-codimension bifurcations of indirect field-oriented control of induction motor. International Journal of Mathematical Models and Methods in Applied Sciences 4: 132-139.
14. Zribi M, Oteafy A, Smaoui N (2009) Controlling chaos in the permanent magnet synchronous motor. Chaos, Solitons and Fractals 41: 1266–1276.
15. Yu J, Chen B, Yu H, Lin C, Ji Z, et al. (2015) Position tracking control for chaotic permanent magnet synchronous motors via indirect adaptive neural approximation. Neuro-computing 156: 245–251.
16. Harb AM (2004) Nonlinear chaos control in a permanent magnet reluctance machine. Chaos, Solitons and Fractals 19: 1217–1224.
17. Dai D, Ma X, Zhang B, Tse CK (2009) Hopf bifurcation and chaos from torus breakdown in voltage-mode controlled DC drive systems. Chaos, Solitons and Fractals 41: 1027–1033.
18. Jing Z, Yu C, Chen G (2004) Complex dynamics in a permanent-magnet synchronous motor model. Chaos, Solitons and Fractals 22: 831–848.
19. Espina J, Arias T, Balcells J, Ortega C (2009) Speed anti-windup PI strategies review for field oriented control of permanent magnet synchronous machines. Compatibility and Power Electronics, CPE2009 6th international conference-workshop.
20. Carcasses JP, Mira C, Bosch M, Simo C, Tatjer JC (1991) Crossroad area–spring area transition (I) parameter plane representation. Int J Bifurcation Chaos.